Available online at www.sciencedirect.com

jmr&t Journal of Materials Research and Technology

journal homepage: www.elsevier.com/locate/jmrt

Short Communication

The unexplored δ-phase of KY_3F_{10}: toward novel Eu^{3+}-doped nanoplates with a 'super-diamond' structure for optical applications

Pablo Serna-Gallén, Héctor Beltrán-Mir[**], *Eloísa Cordoncillo*[*]

Departamento de Química Inorgánica y Orgánica, Universitat Jaume I, Av. Sos Baynat S/n, 12071, Castelló de la Plana, Spain

ARTICLE INFO

Article history:
Received 22 August 2021
Accepted 9 November 2021
Available online 29 November 2021

Keywords:
Crystal Phase
Europium
Luminescent materials
Fluoride
Nanoplates
Sonochemistry

ABSTRACT

This article describes a new, simple, and high-yield method based on a sonochemical process for obtaining the δ-KY_3F_{10}·xH_2O compound with a 'super-diamond' structure, a material that has been completely neglected in the literature since it was first discovered. We explore the mechanism underlying the formation of the synthesized nanomaterials and show their connection with the pH of the medium. Additionally, we demonstrate for the first time the adequacy of the δ-phase of KY_3F_{10} for optical applications through the novel Eu^{3+}-doped nanoplates, which exhibit long lifetimes and high quantum efficiencies. The results reveal that this material, which also has zeolitic characteristics, can have a strong impact on future photonic and associated applications.

1. Introduction

Fluorides doped with luminescent lanthanide ions (Ln^{3+}) are one of the most attractive inorganic materials used for a vast gamut of applications: emitting diodes, up/down-converter phosphors, lasers, catalysts, or biomarkers for in vivo imaging, to name but a few [1–7]. Over the last decade, the KY_3F_{10} structure has received an increasingly large amount of attention due to its photoluminescence features and their associated applications in many fields of materials chemistry [8–12]. Unfortunately, the studies in the literature have only focused on the common α-phase of KY_3F_{10}, a cubic structure with space group (SG) $Fm\bar{3}m$, 8 formula units (Z) per unit cell, and lattice parameter $a = 11.536$ Å [13].

It was not until the year 2000 when a new family of fluorides was discovered by Le Berre et al. [14], who described the structural and crystallographic parameters of the isotypic hydrated δ-phases of $(H_3O)Y_3F_{10}$ and KY_3F_{10}, among others. According to those authors, the compounds were synthesized by adding $Y_2(C_2O_4)_3$·xH_2O (0.7 g) to a heated solution of HF (20 mL of HF 40%) and KF (different [KF]/[Y^{3+}] ratios were used to synthesize the required compound). One aspect that stands out is the amount of hydrofluoric acid (HF) used. It is common

* Corresponding author.
** Corresponding author.
E-mail addresses: mir@uji.es (H. Beltrán-Mir), cordonci@uji.es (E. Cordoncillo).
https://doi.org/10.1016/j.jmrt.2021.11.060

knowledge that HF has an acute toxicity because of its harmful effects and the ability to be readily absorbed through the skin and attack bones [15]. Consequently, the use and handling of HF in the laboratory must be a hazard of concern, and alternative procedures that reduce or eliminate the use of reagents that are harmful to health are a matter of importance.

Since then, little research addressing the δ-(H_3O)$Y_3F_{10}\cdot xH_2O$ structure has appeared in the literature [16–20], the study reported by Caron et al. [18] being the only one that focuses on the properties of this compound for optical applications. Surprisingly, as far as we know, since it was first discovered in 2000, no other additional research has been conducted on the unexplored δ-$KY_3F_{10}\cdot xH_2O$ structure. Moreover, the aforementioned paper of Le Berre et al. did not include any kind of characterization regarding the morphology or size of the material.

δ-$KY_3F_{10}\cdot xH_2O$ has a cubic structure with SG = $Fd\bar{3}m$, $Z = 16$, and a = 15.4917(2) Å [14]. The crystal structure can be described as an association of six YF_8 square antiprisms, called unit of octahedral antiprism (UOA), Fig. 1(a,b). Edge- and corner-shared UOAs are linked to form a three-dimensional cage-like structure with cavities occupied by potassium ions and water molecules, Fig. 1(c). The water molecules can move through the tunnels, conferring a zeolitic behavior on this unique phase. The three-dimensional network can be described as a diamond-type stacking of UOAs, where the central vacancy within each UOA is at the position of a carbon atom in the diamond structure [17,21], Fig. 1(d,e). For comparison purposes, the color of the UOAs in the 'super-diamond' structure view of δ-$KY_3F_{10}\cdot xH_2O$ has been maintained to indicate their respective C atoms.

As per the above considerations, the scope of this publication is to report a simple and high-yield method to obtain the δ-$KY_3F_{10}\cdot xH_2O$ compound. In addition, we study for the first time the growth mechanism of this structure and its perfect adequacy for important optical applications through the novel Eu^{3+}-doped nanoplates. To the best of our knowledge, this is the only research to have contemplated the study of the δ-$KY_3F_{10}\cdot xH_2O$ structure since its original discovery more than twenty years ago. Besides, the alternative method that we present does not require the use of HF and minimizes the safety hazards.

2. Experimental

The novel synthesis of the δ-phase of KY_3F_{10} powders was performed following a sonochemistry approach. Calculations were performed so as to obtain approximately 0.25 g of the final product. In a typical synthesis procedure, 1.5 mmol of $Y(NO_3)_3\cdot 6H_2O$ were dissolved in 30 mL of water with a resulting pH of 4.0. Then, 3.0 mmol of KBF_4 were added to the above solution and the pH of the medium was adjusted to 7.0 by adding dropwise 2 M KOH aqueous solution. The mixture was stirred vigorously for 5 min and the final volume was adjusted to 50 mL with water. The whole system was transferred into a *Bandelin Sonorex* ultrasonic bath operating with a frequency of 35 kHz. After some time, the formation of a white precipitate was observed, while a progressive decrease in the pH was also noted, as will be discussed below. The precipitate was then centrifuged, washed three times with water, and dried under an infrared lamp. The choice of the pH values and their effect on the material is currently under study and will be discussed in a forthcoming publication. The reaction that controls the formation of KY_3F_{10} is highly influenced by the ultrasound-assisted processes that affect the hydrolysis degree of tetrafluoroborate ion. The slow hydrolysis of BF_4^- also depends on the pH (it is favored in basic medium) and implies a large set of reactions that involve complex mechanisms of reaction. Thus, F^- ions are successively released to the medium and react with Y^{3+} and K^+ cations following different pathways to form the corresponding crystal phase. Nevertheless, a comprehensive and accurate approach to fully understand the reaction mechanisms that govern the formation of materials with different structures and morphologies is required and will be the scope of a new study, as previously addressed.

Several samples of the material were prepared according to different reaction times: denoted T2, T4, T6, and T24, with a

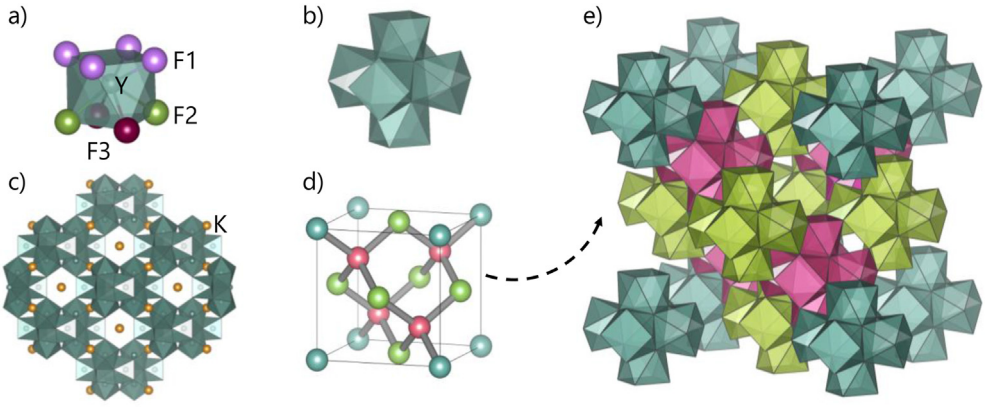

Fig. 1 – (a) YF_8 square antiprism where the F-labels indicate fluoride ions in different Wyckoff positions. (b) Schematic representation of the unit of octahedral antiprism. (c) Three-dimensional cage-like structure with cavities and channels. (d) Corresponding view of the diamond structure with C atoms represented as spheres. (e) 'Super-diamond' structure view of δ-$KY_3F_{10}\cdot xH_2O$.

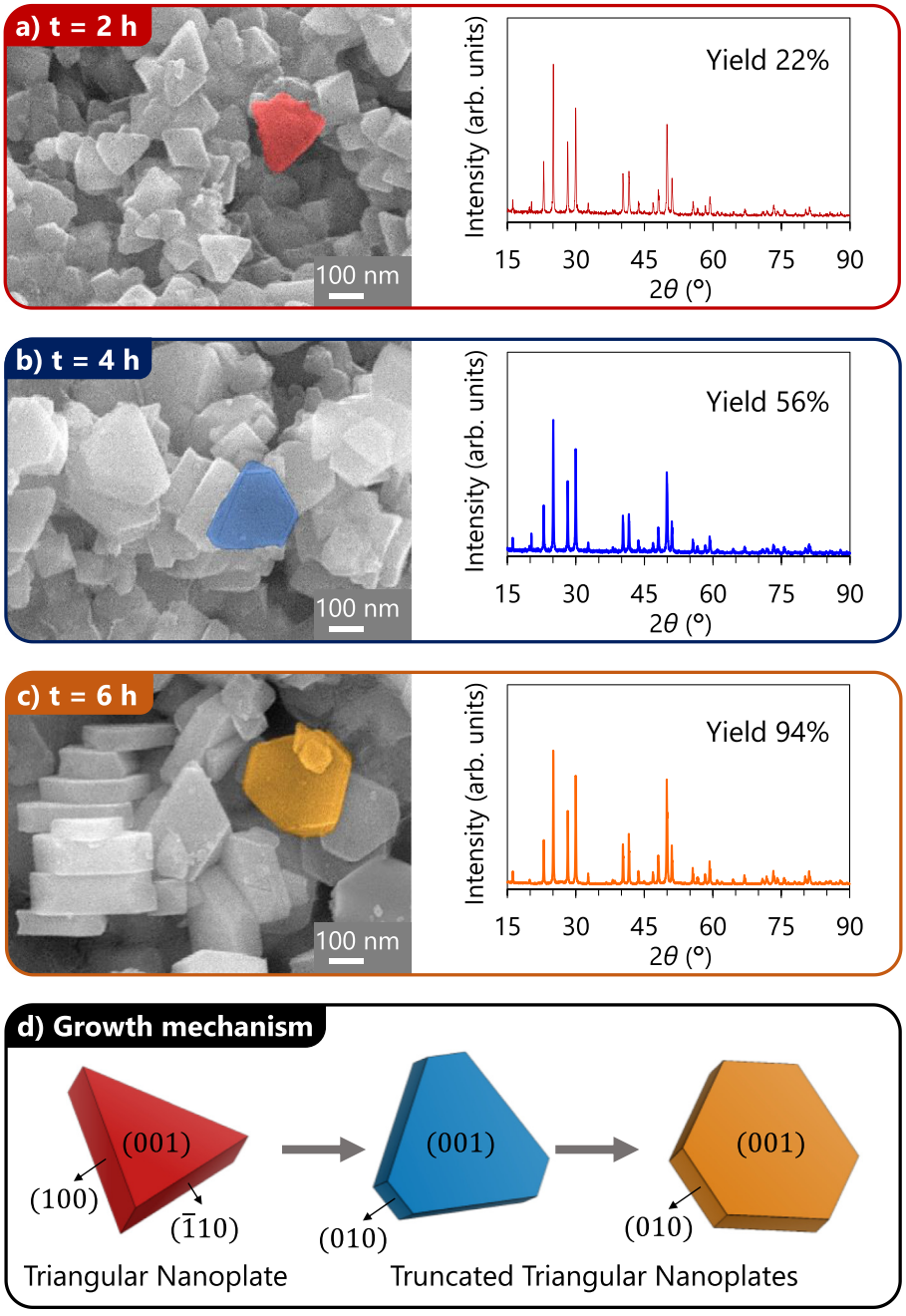

Fig. 2 – SEM images and their respective XRD patterns for samples (a) T2, (b) T4, and T6 (c), which correspond to samples synthesized at different reaction times. For clarity, the ideal morphology has been highlighted in each micrograph. The reaction yields are also indicated as an inset in the XRD patterns. (d) Description of the general growth mechanism along with the evolution of the crystal planes.

reaction time of t = 2, 4, 6, and 24 h, respectively. Moreover, in order to study the photoluminescence properties of the δ-phase of KY_3F_{10} for future photonic applications, we also incorporated the Eu^{3+} ion into the crystal structure (KLn_3F_{10}, Ln = Y, Eu; 1 mol% Eu^{3+}). The nomenclature of this sample was denoted as T6Eu, since the reaction time was 6 h. Further details about the materials and the characterization of the samples can be found in Section 1 of the Supplementary Information.

3. Results and discussion

3.1. *Crystal structure and growth mechanism*

Figure 2 shows the SEM images and their respective XRD patterns for samples (a) T2, (b) T4, and (c) T6, which correspond to samples synthesized at different reaction times. The reaction yields are also indicated as an inset in the XRD

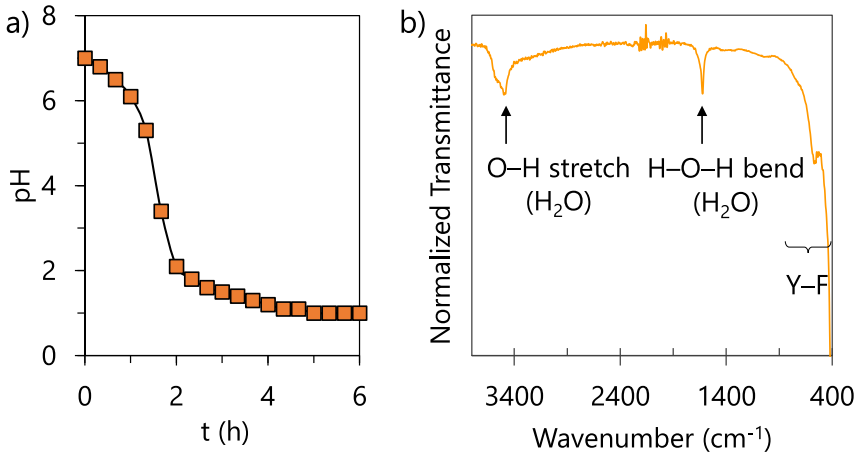

Fig. 3 – (a) Evolution of the pH of the reaction medium with time. (b) FT-IR spectrum of sample T6.

patterns. The Eu^{3+}-doped sample (T6Eu, not shown) presented the same structural and morphological characteristics as T6. Sample T24 has been omitted throughout the paper because no improvement in the reaction yield nor any noticeable changes in the morphology/size and XRD pattern were appreciated, suggesting that the reaction is already completed within 6 h. Thus, the crystal and thermal analyses were performed with sample T6, which reached the maximum reaction yield (94%).

The XRD patterns show all the peaks corresponding to δ-$KY_3F_{10}\cdot xH_2O$ (ICDD card 04-016-7073) [22]. All samples exhibit narrow, high-intensity peaks, meaning that the materials are fairly crystalline. The refined crystal parameters of sample T6 (a = 15.4934(5) Å, V = 3719.12(21) $Å^3$) are also in good agreement with those reported for the structure.

For the interpretation of the growth mechanism, Fig. 2(d), the ideal morphology of the majority of the particles was computer-simulated indicating the corresponding crystal planes of the different facets. The proposed mechanism can be well explained through the evolution of triangular nanoplates with time toward the formation of truncated triangular nanoplates by the gradual growth of (010) planes. We also noted that the aggregation of some particles occurred in order to reduce their surface energy. The mechanism is fairly correlated with the pH of the reaction medium, as highlighted in Fig. 3(a). At ≈ 1.5 h (which coincides with the inflection point of the curve) the formation of an incipient precipitate was observed. With the evolution of the reaction time, the amount of precipitate increased (see the reaction yields) and the morphology of samples changed while a progressive decrease in the pH was observed until a value of 1.1 was reached.

To further confirm the formation of the desired compound instead of the δ-$(H_3O)Y_3F_{10}\cdot xH_2O$ structure, the potassium-yttrium proportion was measured by ICP-MS, an approximate atomic ratio of (0.9)K(3.0)Y being obtained, which is in perfect agreement with the stoichiometry of the crystal structure. Moreover, the FT-IR spectrum, Fig. 3(b), shows the common stretching and bending vibrational modes of the crystalline water molecules, as well as the Y–F host lattice vibrations below 600 cm^{-1}.

3.2. *Thermal analysis*

TG/DSC experiments of sample T6 allowed us to study the thermal behavior of the nanomaterials, Fig. 4. The compound exhibits a progressive loss of mass (6.65%), which is associated with the crystalline water present in the δ-$KY_3F_{10}\cdot xH_2O$ structure. According to these data, the number of water molecules was established to be x = 1.96 (≈2). Thus, to obtain the reaction yields (see the previous section), the compound was considered to be δ-$KY_3F_{10}\cdot 2H_2O$. The absence of multiple or notable (endo/exo)thermic peaks in the temperature range 25–300 °C also highlights the fact that there are no apparent traces of a possible δ-$(H_3O)Y_3F_{10}\cdot xH_2O$ phase. The exothermic peak found at 439.2 °C is associated with the δ-KY_3F_{10} → α-KY_3F_{10} transition [14].

The enthalpy corresponding to this transition (ΔH = – 25.5 kJ/mol) was calculated from the experimental data taking into account the area of the exothermic peak, the heat flow, and considering the δ-$KY_3F_{10}\cdot 2H_2O$ stoichiometry for the initial mass of the sample. The exothermic process has been expressed with a negative ΔH value by the usual convention in thermodynamics.

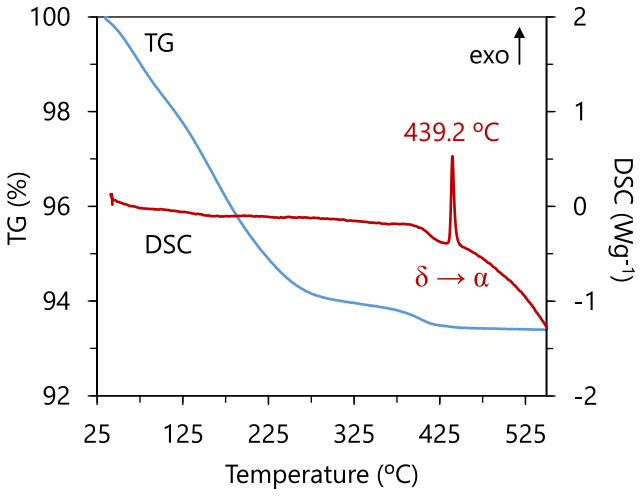

Fig. 4 – TG/DSC curves for sample T6.

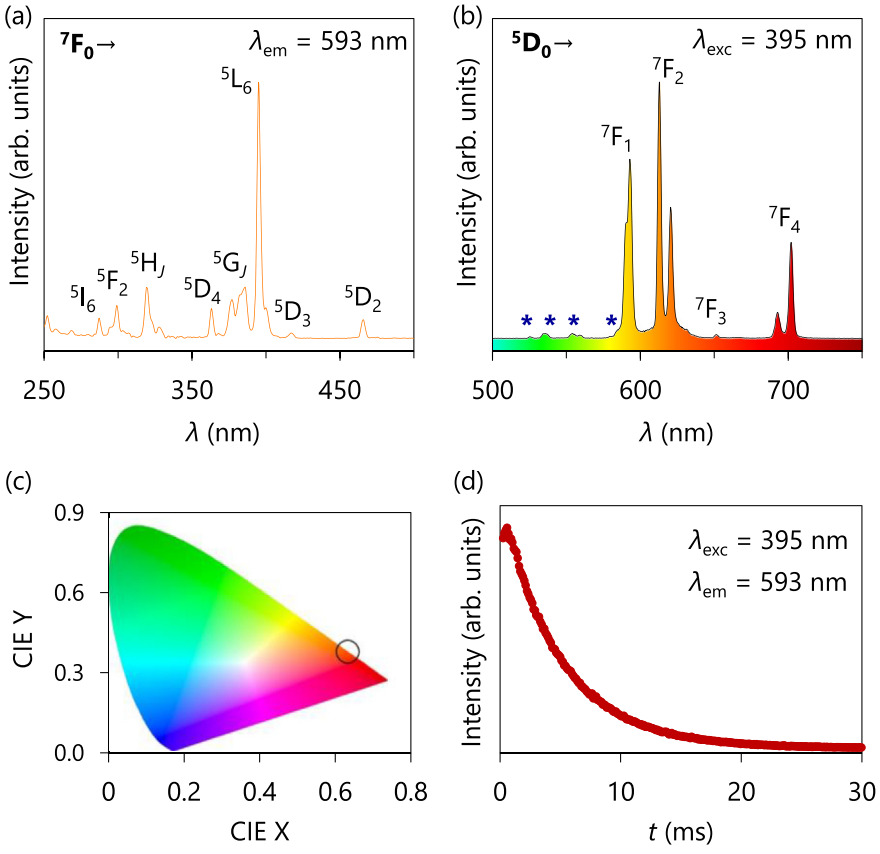

Fig. 5 – Room temperature photoluminescent studies of sample T6Eu obtained with a DT of 0.2 ms: (a) excitation and (b) emission spectra, (c) CIE chromaticity diagram, and (d) decay curve. The blue stars in (b) correspond to a small contribution of $^5D_1\rightarrow{}^7F_J$ transitions.

3.3. *Photoluminescence studies*

The photoluminescence studies were conducted on the Eu^{3+}-doped sample (T6Eu), which incorporates the Eu^{3+} ion into the crystal structure of the material (KLn_3F_{10}, Ln = Y, Eu; 1 mol% Eu^{3+}). The similarity between the ionic radius of Y^{3+} (1.019 Å for a coordination number, CN, = 8) and Eu^{3+} (1.066 Å for a CN = 8) [23] ensures perfect incorporation of the Eu^{3+} ions in the host lattice. See Fig. 1(a) for a better comprehension of the CN.

Regarding the excitation spectrum of sample T6Eu, Fig. 5(a), different bands associated with the Eu^{3+} transitions were observed from the ground level $^7F_0$ to the different excited levels. Among all the transitions, the most intense was $^7F_0\rightarrow{}^5L_6$, with a maximum at 395 nm. Therefore, the emission spectrum of this powder was recorded using this value as the excitation wavelength.

Figure 5(b) shows the emission spectrum obtained with a delay time (DT) of 0.2 ms and the typical bands corresponding to the $^5D_0\rightarrow{}^7F_J$ transitions of Eu^{3+}. The blue stars are associated with a small contribution of $^5D_1\rightarrow{}^7F_J$ transitions. With the aim of suppressing the contribution of the latter transitions to subsequent calculations of some optical parameters, the emission spectrum was also recorded with a DT = 10 ms. A comparison between the emission spectrum of sample T6Eu recorded at DT = 0.2 and 10 ms can be found in Fig. S1.

The CIE chromaticity diagram is depicted in Fig. 5(c), highlighting the orange-reddish color emission of the nanoplates. Additionally, the Eu^{3+}-doped powders were studied by time-resolved phosphorescence spectroscopy. The observed lifetime (τ_{obs}) of the $^5D_0$ excited level was extracted from the decay curve corresponding to the $^5D_0\rightarrow{}^7F_1$ transition, Fig. 5(d), and the quantum efficiency (the intrinsic quantum yield, η) of the material was also calculated.

On the other hand, for the particular case of the Eu^{3+} ion, several physicochemical parameters can be determined directly from the analysis of the emission spectra. The asymmetry ratio R is useful to analyze the local symmetry of the dopant and is defined as the ratio between the intensities of the $^5D_0\rightarrow{}^7F_2$ (electric dipole) and $^5D_0\rightarrow{}^7F_1$ (magnetic dipole) transitions. The Ω_2 Judd–Ofelt parameter is related to the polarizable and covalent character of the lanthanide ion in the lattice associated with the crystal environment, while the Ω_4 Judd–Ofelt parameter is sensitive to the rigidity of the crystal lattice, which is a long-range effect [24,25]. Table 1 lists the values of R, Ω_2, Ω_4, τ_{obs}, and η for sample T6Eu (δ-$KY_3F_{10}\cdot xH_2O$ structure). For further explanations about the calculations of

Table 1 – Photoluminescent parameters for the Eu^{3+}-doped δ-$KY_3F_{10}·xH_2O$ crystal structure.

R	Ω_2 (10^{-20} cm^2)	Ω_4 (10^{-20} cm^2)	Ω_2/Ω_4	τ_{obs} (ms)	η (%)
1.46	2.57(3)	1.94(2)	1.32	4.96(1)	70

the previous parameters, see Section 3 of the Supplementary Information.

The value of *R* is in agreement with the dominance of the electric dipole transition in the emission spectrum and evidences the existence of some asymmetry around Eu^{3+} ions. The Ω_2/Ω_4 ratio also suggests that Eu^{3+} ions are mostly localized in symmetry sites with some degree of distortion [26]. In addition, the nanoparticles exhibit long lifetimes (≈5 ms) and high quantum efficiencies (70%).

As stated earlier, Caron et al. studied the optical properties of Eu^{3+}-doped δ-$(H_3O)Y_3F_{10}·xH_2O$ compounds [18]. Although the values of *R* and the Judd–Ofelt parameters were not reported in their study, a qualitative interpretation can be made from the emission spectra (Figure 7 of their publication) because these parameters are directly related to the intensity of $^5D_0 \rightarrow {}^7F_J$ transitions (see equations S1 and S2 of the Supplementary Information). In comparison with the emission spectrum of sample T6Eu (this work), the relative intensities of $^5D_0 \rightarrow {}^7F_1$ and $^5D_0 \rightarrow {}^7F_2$ transitions seem to be similar, while the intensity of the $^5D_0 \rightarrow {}^7F_4$ transition is clearly higher. Thus, similar values of *R* and Ω_2, and a higher value of Ω_4 are expected for Eu^{3+}-doped δ-$(H_3O)Y_3F_{10}·xH_2O$ compounds. These remarks lead us to believe that europium has comparable crystal environments when doping δ-$KY_3F_{10}·xH_2O$ and δ-$(H_3O)Y_3F_{10}·xH_2O$ structures, since in both cases Eu^{3+} occupies the crystallographic position of Y^{3+}. The differences expected in Ω_4 can be attributed to the different host lattices, as it is a long-range parameter.

In any case, the nanoparticles of this work exhibit longer lifetimes (≈5 ms) than those of Caron et al. [18], which obtained a lifetime of 3.20(9) ms with a similar Eu^{3+} concentration for the δ-$(H_3O)Y_3F_{10}·xH_2O$ structure. This improvement might be well attributed to the presence of K^+ ions in the host lattice instead of hydroniums, which could partially quench the luminescence. Therefore, the novel nanomaterials could find interesting applications in photonics.

4. Conclusions

This work presents a new, simple, and high-yield method to synthesize the δ-phase of KY_3F_{10}. In order to shed some light on the formation of the truncated triangular nanoplates, the growth mechanism has been studied, the results showing a strong dependence on the pH of the medium. We have also explored for the first time the photoluminescence features of the Eu^{3+}-doped nanomaterials of this structure. The electric dipole transition domination over the emission spectrum results in an orangish emission of the powders. The zeolitic character of this structure and the unique site–sensitive properties of Eu^{3+} make these materials potentially useful candidates as probes in detection or imaging applications. At the same time, the optical analysis underscores their good suitability for photonics, which could arouse widespread interest among the scientific community.

Declaration of Competing Interest

The authors declare that they have no known competing financial interests or personal relationships that could have appeared to influence the work reported in this paper.

Acknowledgments

The authors thank the Universitat Jaume I (Project UJI-B2019-41) for financial support. P. Serna also thanks the Spanish Ministerio de Ciencia, Innovación y Universidades for an FPU predoctoral contract.

Appendix A. Supplementary data

Supplementary data to this article can be found online at https://doi.org/10.1016/j.jmrt.2021.11.060.

REFERENCES

[1] Sassoye C, Patriarche G, Mortier M. High yield syntheses of reactive fluoride $K_{1-x}(Y, Ln)_xF_{1+2x}$ nanoparticles. Opt Mater 2009;31:1177–83. https://doi.org/10.1016/j.optmat.2008.12.013.

[2] Wu J, Wang J, Lin J, Xiao Y, Yue G, Huang M, et al. Dual functions of YF_3:Eu^{3+} for improving photovoltaic performance of dye-sensitized solar cells. Sci Rep 2013;3:1–5. https://doi.org/10.1038/srep02058.

[3] Tissue BM. Synthesis and luminescence of lanthanide ions in nanoscale insulating hosts. Chem Mater 1998;10:2837–45. https://doi.org/10.1021/cm9802245.

[4] Grzyb T, Węcławiak M, Pędziński T, Lis S. Synthesis, spectroscopic and structural studies on YOF, LaOF and GdOF nanocrystals doped with Eu^{3+}, synthesized via stearic acid method. Opt Mater 2013;35:2226–33. https://doi.org/10.1016/j.optmat.2013.06.007.

[5] Deng M, Ma Y, Huang S, Hu G, Wang L. Monodisperse upconversion $NaYF_4$ nanocrystals: syntheses and bioapplications. Nano Res 2011;4:685–94. https://doi.org/10.1007/s12274-011-0124-y.

[6] Podhorodecki A, Noculak A, Banski M, Sojka B, Zelazo A, Misiewicz J, et al. Lanthanides fluorides doped nanocrystals for biomedical applications. ECS Trans 2014;61:115–25. https://doi.org/10.1149/06105.0115ecst.

[7] Jain A, Fournier PGJ, Mendoza-Lavaniegos V, Sengar P, Guerra-Olvera FM, Iñiguez E, et al. Functionalized rare earth-doped nanoparticles for breast cancer nanodiagnostic using fluorescence and CT imaging. J Nanobiotechnol 2018;16:1–18. https://doi.org/10.1186/s12951-018-0359-9.

[8] Zhu L, Meng J, Cao X. Sonochemical synthesis of monodispersed KY_3F_{10}:Eu^{3+} nanospheres with bimodal size distribution. Mater Lett 2008;62:3007–9. https://doi.org/10.1016/j.matlet.2008.01.096.

[9] Cao C. Hydrothermal synthesis, phase evolution, and optical properties of Eu^{3+}-doped KF-YF_3 system materials. J Mater Res Soc 2012;27:2988–95. https://doi.org/10.1557/jmr.2012.331.

[10] Goderski S, Runowski M, Lis S. Synthesis of luminescent KY_3F_{10} nanopowder multi-doped with lanthanide ions by a co-precipitation method. J Rare Earths 2016;34:808–13. https://doi.org/10.1016/S1002-0721(16)60098-4.
[11] Runowski M. Color-tunable up-conversion emission of luminescent-plasmonic, core/shell nanomaterials - KY_3F_{10}:Yb^{3+},Tm^{3+}/SiO_2-NH_2/Au. J Lumin 2017;186:199–204. https://doi.org/10.1016/j.jlumin.2017.02.032.
[12] Chen M, Loiko P, Serres JM, Veronesi S, Tonelli M, Aguiló M, et al. Fluorite-type Tm^{3+}:KY_3F_{10}: a promising crystal for watt-level lasers at ~1.9 μm. J Alloys Compd 2020;813:152176. https://doi.org/10.1016/j.jallcom.2019.152176.
[13] Villars P, Cenzual K, editors. KY_3F_{10} Crystal Structure: Datasheet from 'PAULING FILE Multinaries Edition – 2012' in Springer Materials (https://materials.springer.com/isp/crystallographic/docs/sd_0552093).
[14] Le Berre F, Boucher E, Allain M, Courbion G. Synthesis, stability and zeolitic behavior of δ-ALn_3F_{10},xH_2O and γ-$ThLn_2F_{10}$,H_2O phases (Ln=lanthanide). J Mater Chem 2000;10:2578–86. https://doi.org/10.1039/b002520h.
[15] Harris J, Minor P, Chawla N, Singh S. Development and implementation of a hydrofluoric acid safety program in an academic institution. ACS Chem Heal Saf 2020;27:183–9. https://doi.org/10.1021/acs.chas.0c00008.
[16] Fedorov PP, Mayakova MN, Kuznetsov SV, Voronov VV, Ermakov RP, Samarina KS, et al. Co-precipitation of yttrium and barium fluorides from aqueous solutions. Mater Res Bull 2012;47:1794–9. https://doi.org/10.1016/j.materresbull.2012.03.027.
[17] Lucier BEG, Johnston KE, Arnold DC, Lemyre JL, Beaupré A, Blanchette M, et al. Comprehensive solid-state characterization of rare earth fluoride nanoparticles. J Phys Chem C 2014;118:1213–28. https://doi.org/10.1021/jp408148b.
[18] Caron C, Boudreau D, Ritcey AM. Luminescent properties of europium-doped $(H_3O)Y_3F_{10}\cdot xH_2O$ nanocrystals. J Mater Chem C 2015;3:9955–63. https://doi.org/10.1039/c5tc02527c.
[19] Richard B, Lemyre JL, Ritcey AM. Nanoparticle size control in microemulsion synthesis. Langmuir 2017;33:4748–57. https://doi.org/10.1021/acs.langmuir.7b00773.
[20] Andrrev OV, Razumkova IA, Boiko AN. Synthesis and thermal stability of rare earth compounds REF_3, $REF_3\cdot nH_2O$ and $(H_3O)RE_3F_{10}\cdot nH_2O$ (RE = Tb – Lu, Y), obtained from sulphide precursors. J Fluor Chem 2018;207:77–83. https://doi.org/10.1016/j.jfluchem.2017.12.001.
[21] Stephens NF, Lightfoot P. An organically templated yttrium fluoride with a 'Super-Diamond' structure. J Solid State Chem 2007;180:260–4. https://doi.org/10.1016/j.jssc.2006.09.032.
[22] Villars P, Cenzual K, editors. δ-$KY_3F_{10}\cdot xH_2O$ ($KY_3F_{10}[H_2O]$) Crystal Structure: Datasheet from 'PAULING FILE Multinaries Edition – 2012' in Springer Materials (https://materials.springer.com/isp/crystallographic/docs/sd_1004004).
[23] Shannon RD. Revised effective ionic radii and systematic studies of interatomic distances in halides and chalcogenides. Acta Crystallogr 1976;A32:751–67. https://doi.org/10.1107/S0567739476001551.
[24] Patel DK, Vishwanadh B, Sudarsan V, Kulshreshtha SK. Difference in the nature of Eu^{3+} environment in Eu^{3+}-doped $BaTiO_3$ and $BaSnO_3$. J Am Ceram Soc 2013;96:3857–61. https://doi.org/10.1111/jace.12596.
[25] de Mello Donegá C, Junior SA, de Sá GF. Synthesis, luminescence and quantum yields of Eu(III) mixed complexes with 4,4,4-trifluoro-1-phenyl-1,3-butanedione and 1,10-phenanthroline-N-oxide. J Alloys Compd 1997;250:422–6. https://doi.org/10.1016/S0925-8388(96)02562-5.
[26] Cantelar E, Sanz-García JA, Sanz-Martín A, Muñoz Santiuste JE, Cussó F. Structural, photoluminescent properties and Judd-Ofelt analysis of Eu^{3+}-activated CaF_2 nanocubes. J Alloys Compd 2020;813:152194. https://doi.org/10.1016/j.jallcom.2019.152194.